Frequency-time spectra of magnetospherically reflecting whistlers in the plasmasphere

J. Bortnik, U. S. Inan, and T. F. Bell

Space, Telecommunications, and Radioscience Laboratory, Electrical Engineering Department, Stanford University, Palo Alto, California, USA

Received 14 March 2002; revised 20 September 2002; accepted 26 September 2002; published 23 January 2003.

[1] We present a numerical method of simulating at any location in the magnetosphere, the observed frequency versus time (*f-t*) spectrogram resulting from a lightning strike at any given latitude on Earth. Using a two-dimensional ray tracing code, we calculate the trajectories of 5330 whistler rays that effectively sample the lightning strike's frequency spectrum and latitudinal spread about the source and then use these so-called "sample rays" to create ~120 million interpolated rays, each weighted with a measure of energy according to its frequency and injection latitude. This energy is progressively attenuated along the ray's trajectory using a Landau damping calculation with realistic suprathermal electron fluxes. A detection area is defined in the plasmasphere, and rays that cross this area are used to construct the *f-t* spectrogram representative of what would be observed on a satellite located in that region. We investigate the role that the lightning source latitude, observation location, and plasmaspheric electron density structures have on the appearance of the simulated *f-t* spectrograms and show that all three parameters exhibit distinct and well-defined effects. In particular, we focus on plasmaspheric electron density structures and explain the connection between these structures and the appearance of specific observed features in the spectrograms. Using this analysis, it may be possible to crudely infer certain features of the source and plasmasphere from observed magnetospherically reflecting whistler spectrograms. *INDEX TERMS:* 6964 Radio Science: Radio wave propagation; 6939 Radio Science: Magnetospheric physics; 7843 Space Plasma Physics: Numerical simulation studies; 7871 Space Plasma Physics: Waves and instabilities; *KEYWORDS:* magnetospherically reflecting, nonducted, whistlers, plasmasphere, VLF, spectrograms

Citation: Bortnik, J., U. S. Inan, and T. F. Bell, Frequency-time spectra of magnetospherically reflecting whistlers in the plasmasphere, *J. Geophys. Res.*, *108*(A1), 1030, doi:10.1029/2002JA009387, 2003.

1. Introduction

[2] Magnetospherically reflecting (MR) whistlers have been studied by numerous authors [*Kimura*, 1966; *Smith and Angerami*, 1968; *Edgar*, 1976; *Sonwalker and Inan*, 1988; *Draganov et al.*, 1992, 1993; *Thorne and Horne*, 1994; *Shklyar and Jiříček*, 2000] ever since they were first observed aboard the OGO1 and OGO3 satellites [*Smith and Angerami*, 1968]. The generally accepted phenomenology of MR whistlers is as follows: a lightning strike radiates electromagnetic energy in the ELF and VLF frequency bands which propagates away from the source within the Earth-ionosphere waveguide [*Crary*, 1961]. At the bottomside ionosphere a portion of the radiation leaks upward out of the Earth-ionosphere waveguide and into the ionosphere where it propagates in the whistler mode [*Edgar*, 1976]. Owing to the sharp positive gradients in electron number density, the wave normal angles of these upward propagating whistler mode waves are refracted as they traverse the ionosphere and become approximately vertical at the top of the *F* region [*James*, 1972]. Beyond this altitude, the wave normal angles are gradually refracted away from the vertical direction due to the negative vertical gradient in electron density, the prevailing horizontal electron density gradients, as well as the local magnetic field gradient and curvature [*James*, 1972]. In traversing the ionosphere, the power density of the wave is attenuated owing to collisional losses such that wave intensities are reduced by as much as ~3 dB during nighttime and ≥20 dB under daytime ionospheric conditions [*Helliwell*, 1965, p. 67].

[3] By the time it has entered the plasmasphere, the VLF radiation has permeated a large region surrounding the source [*Lauben et al.*, 1999; *Inan et al.*, 1984], and it propagates away from the Earth and is guided by the plasmaspheric electron density and magnetic field gradients. The ray paths initially tend not to deviate substantially from the geomagnetic field lines and are eventually bent toward lower altitudes. Considering the dispersion relation with the inclusion of ions, *Kimura* [1966] was the first to predict that such Earthward moving whistlers could, under some conditions, have their wave normal angles refracted past 90° such that the group velocity would reverse direction, and the wave would, in effect, magnetospherically reflect and begin

0148-0227/03/2002JA009387$09.00

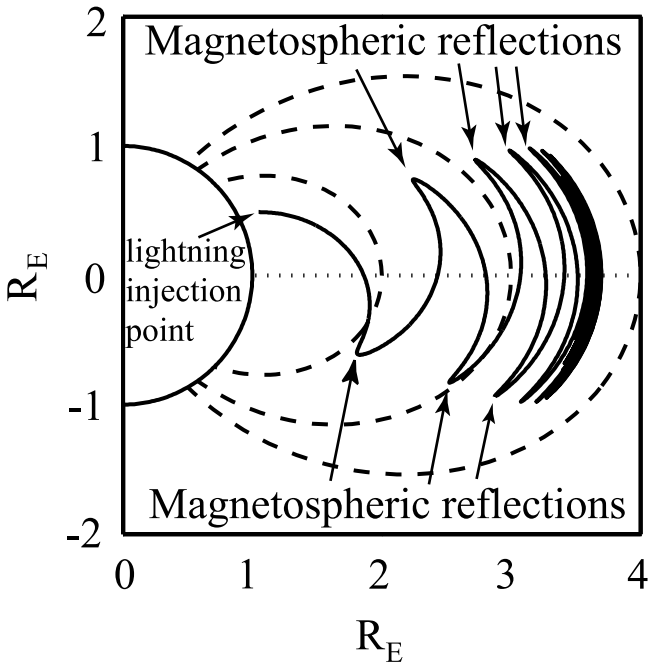

Figure 1. Ray trajectory of a typical MR whistler wave, showing points of magnetospheric reflection, and injection latitude (f = 0.5 kHz, λ = 25°).

moving in roughly the opposite direction. A typical ray path calculated using the Stanford VLF raytracing code [*Inan and Bell*, 1977] is shown in Figure 1, and an example of an MR whistler observed aboard the OGO 1 satellite is shown in Figure 2a (from *Smith and Angerami* [1968]).

[4] The subject of MR whistlers has recently come to the fore as a result of observations of the precipitation of radiation belt electrons by nonducted, obliquely propagating whistler waves launched by lightning discharges [*Lauben et al.*, 1999; *Johnson et al.*, 1999] and specifically by MR whistlers [*Blake et al.*, 2001]. Theoretical considerations of MR whistler-induced precipitation have so far included only preliminary assessments [*Jasna et al.*, 1992; J. Bortnik et al., Energy distribution and lifetime of magnetospherically reflecting whistlers in the plasmasphere, submitted to *Journal of Geophysical Research*, 2002, hereinafter referred to as Bortnik et al., submitted manuscript, 2002] primarily owing to the recognition of the complexity of the space-time distributions of MR whistler wave energy in the magnetosphere.

[5] In the present work we compute the trajectories of rays originating from a single lightning strike at a given source latitude and calculate the frequency-time spectra of MR whistlers as they would be observed at a variety of locations in the plasmasphere. We use suprathermal electron fluxes observed on the HYDRA instrument aboard the POLAR satellite [*Bell et al.*, 2002] to estimate the Landau damping experienced by each ray along its path, quantitatively determining the frequency-time distributions of wave energy at different locations in the plasmasphere.

[6] We utilize an interpolation scheme, effectively tracing over 100 million rays to represent the wave energy injected by a given lightning strike, thus producing spectrograms exhibiting realistic frequency versus time (f-t) features, with expected power levels (specified in dB relative to 1 pW/m^2/Hz) at any given point in the plasmasphere. We further examine the effects of different plasmaspheric electron density profiles on the observed f-t features and wave power levels. Our results indicate that the various electron density profiles lead to distinct and easily recognizable spectral signatures suggesting that it may be possible to crudely infer the underlying electron density structure in the plasmasphere by observing an MR whistler echo train at a given location in the plasmasphere.

2. Description of the Model

[7] To represent the plasmaspheric distribution of VLF waves due to a single lightning strike, the trajectories of 41 rays injected over a ±10° geomagnetic latitude range about the source are numerically computed for each frequency component using the two-dimensional Stanford VLF raytracing code [*Inan and Bell*, 1977]. For example, to simulate a lightning source latitude of 35°, rays are injected over the range of 25° to 45° spaced 0.5° apart in latitude.

[8] Each injected ray is initially assigned a power density (discussed in section 2.1) consistent with the lightning frequency spectrum, the attenuation experienced by the wave during propagation in the Earth-ionosphere waveguide, and the subsequent trans-ionospheric propagation loss. To represent the full lightning spectrum, 130 frequencies spaced approximately logarithmically between 200 Hz and 60 kHz are computed. The resulting 5330 rays thus form the "sample rays" between which interpolation is performed as described in section 2.2. The Landau damping of each sample ray is calculated along its trajectory, and the wave energy represented by the rays that cross a given magnetospheric location is recorded and used in the construction of the frequency-time spectrogram at that observation point. The calculation procedure is discussed in greater detail in the following subsections.

2.1. Wave Power Density at the Point of Injection of Rays

[9] To compute the wave power density at the injection altitude (1000 km) and latitude of the whistler rays, we use the same methodology employed by Bortnik et al. (submitted manuscript, 2002), summarized here for convenience. The wave power density at a free-space distance R from a lightning source is derived from the expression given by *Uman* [1984, p. 61] for the lightning-radiated electric field, together with a model for the discharge current profile given by *Cummer and Inan* [1997], resulting in the expression

$$S(\omega) = \frac{1}{Z_0}\left(\frac{\mu_0 h_e I_0}{2\pi}\right)^2 \left(\frac{\sin\theta}{R}\right)^2 \frac{\omega^2 (a-b)^2}{(\omega^2+a^2)(\omega^2+b^2)}, \qquad (1)$$

where $S(\omega)$ is the power spectral density in W/m^2/Hz, ω is the radial frequency of the electromagnetic wave in rad/sec, Z_0 and μ_0 are the impedance (≈377 Ω) and permeability of free space (≈8.854 × 10^{-12} F/m), respectively, θ and R are the angle of the observer with respect to the local zenith and the distance of the observer from the lightning source respectively, h_e is the height of the cloud above ground (set to 5 km), I_0 is the magnitude of the downward moving current (set to −10.53 kA), and a, b are model parameters

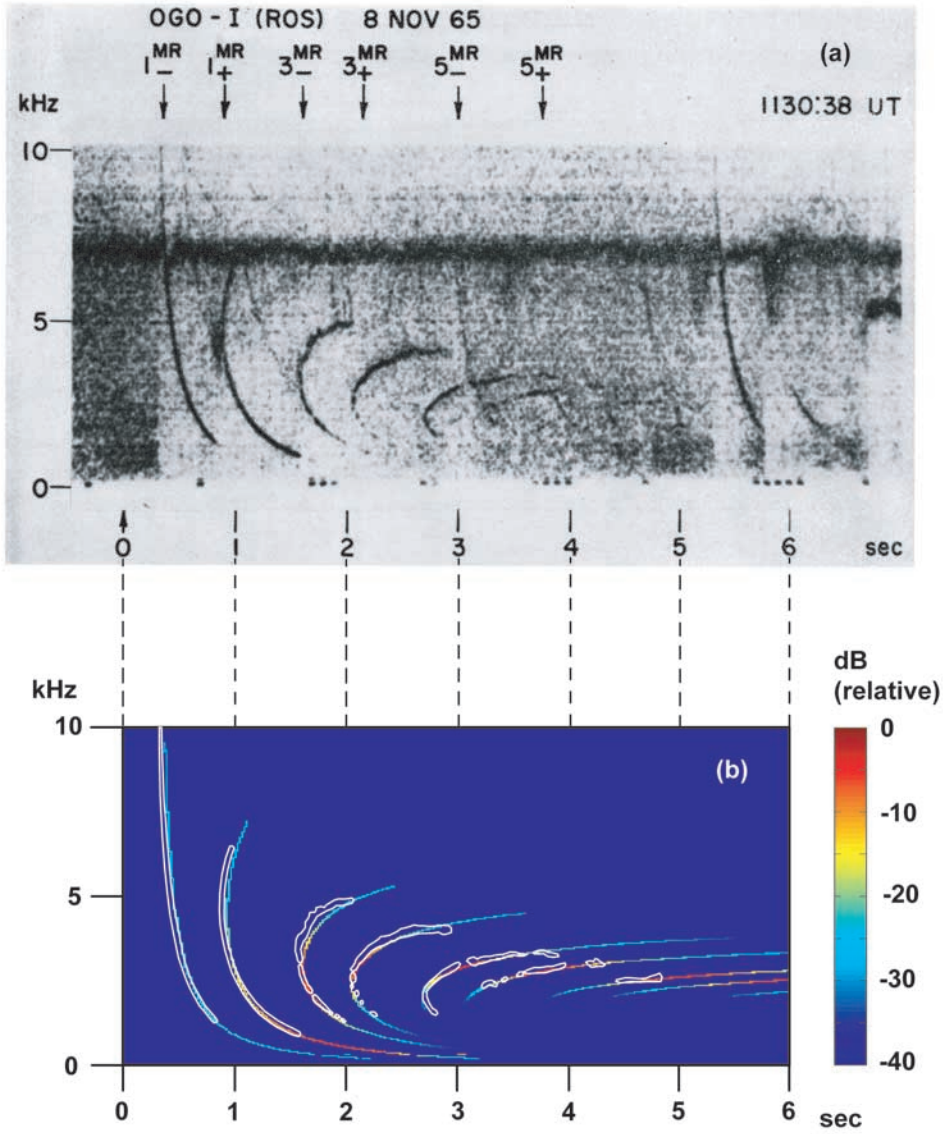

Figure 2. (a) Example of an MR whistler echo train observed aboard the OGO 1 satellite at $L = 2.4$ and $\lambda = 5°$S, and (b) a simulated spectrogram at the same location with a scale overlay of the MR whistler components of Figure 2a.

set to 5×10^3 and 1×10^5, respectively, to give an electric field amplitude of 10 V/m at 100 km. Although this relation is derived for free space, it is adopted here on the basis that the attenuation of VLF wave energy in the Earth-ionosphere waveguide has been shown to be quite similar [*Crary*, 1961] for distances within ≈1000 km from the source.

[10] Using equation (1), the wave power density along the bottomside ionosphere (assumed to be at 100 km altitude) is computed for the region surrounding the source. It should be mentioned that equation (1) predicts a radiation pattern null directly above the lightning source, which is likely washed out owing to inhomogeneities in the ionosphere as evidenced by the lack of such a null in satellite observations of wave power distributions above fixed sources, such as VLF transmitters which utilize electrically short vertical monopole antennas [*Inan et al.*, 1984]. Noting that the artificial imposition of such a null would distort the magnetospheric wave power distribution, we assume the source to be slightly displaced in longitude (0.7°) from the meridian of interest thereby avoiding the radiation pattern null.

[11] The computed wave power density at 100 km altitude is translated to ∼1000 km altitude by properly attenuating it with a factor taken from *Helliwell* [1965, Figures 3–35]. This procedure results in an array $S(f, \lambda, \lambda_s)$, the entries of which are dependent on the frequency (f) and latitude (λ) representing wave power density at 1000 km due to a lightning strike at a source latitude λ_s.

[12] Since we are considering a transient impulsive signal injected by a lightning discharge, we take each ray to carry a portion of energy in accordance with the frequency spectrum in equation (1). For this purpose the initial wave power density represented by each ray is integrated with respect to space, frequency, and time. For spatial integration we multiply the wave power density by the latitudinal extent of the ray converted to units of distance. The latitudinal extent follows from the number of rays injected per degree

of latitude and hence the latitudinal range that each ray is intended to represent. Since we are using two-dimensional ray tracing, instead of integrating the wave power with respect to some longitudinal extent, we assume azimuthal symmetry and let the wave energy density (i.e., energy per meter of longitudinal arc length) vary in inverse proportion to the arc length of the thin longitudinal slice in which we assume the wave energy to be contained. In a similar way, integration with respect to frequency is carried out by multiplying the intensity of each frequency component as calculated by equation (1), with the bandwidth that it is intended to represent. Time integration was performed by assuming that the power of each frequency component was initially constant over a period of 200 μs, and zero otherwise, consistent with a typical lightning waveform [*Uman*, 1984, chapter 4]. It is important to note that in both frequency and time, the above-mentioned integration is performed after interpolation between sample rays has been carried out.

2.2. Detection of Whistler Waves at an Observation Point

[13] Before proceeding to the discussion of interpolation between rays, it is instructive to first consider how such rays will be detected in our simulation. For this purpose we define a small detection area oriented along the magnetic equatorial plane having a given *L*-shell extent (see below). After every time step in the course of our ray-tracing calculations, we check whether either of the sample rays or interpolated rays has crossed the detection area. If so, a few key parameters of the ray are recorded into a file, such as the time of crossing, frequency of the ray, injection latitude, wave energy carried by the ray, and wave normal angle.

[14] The key parameter to be chosen is the extent of the detection area along the magnetic equatorial plane. This choice is bounded by the following two constraints: if the detection area is chosen to be too small, there will not be a sufficiently large number of rays crossing it to subsequently produce a meaningful *f-t* spectrogram. If on the other hand, it is too large, we will no longer be representing the wave spectrum as observed at a "single" point in space but a region over which our measured quantity does not necessarily remain uniform. The net effect of a detection area that is too large will be a "smearing" of the spectrogram in both frequency and time. This smearing can be understood if we consider a wave front at a particular frequency (say f_H, as shown in Figure 3b, in connection with the interpolation discussion) impinging obliquely upon the detection area oriented along the magnetic equator. The smearing in time will depend on the difference in arrival times of the first and last ray to cross the detection area. If the detection area is large, this time difference will also be large. In fact, this time smearing is unavoidable and will occur no matter how small we choose the detection area to be (assuming it has a finite extent); the criteria which we employ is to select the time smearing to be much smaller than the width of the time-bin used to construct our spectrogram. We briefly note in this connection that the resolution we choose for the Δf-Δt bins in our frequency-time spectrograms sets an upper limit on the size of the detection area we employ to detect the rays, and this size, in turn, dictates the number of rays necessary for the simulation (i.e., we need to trace more ray paths if the detection area is small, to ensure that a sufficiently large number of rays cross it) and hence the degree of interpolation.

[15] The detection area chosen for the present simulation was ~5 km (~0.0008 *L*) in extent, ensuring a resolution of $\Delta t < 7$ ms in the spectrogram. We note that in launching the rays, the wave energy represented by each ray was determined by integration over its latitudinal extent. Since we use two-dimensional ray tracing, we account for wave-energy spreading in the azimuthal direction by assuming azimuthal symmetry and hence that the wave energy is contained within a thin longitudinal slice. The energy density (i.e., Joules per meter of longitudinal arc length) carried by each ray thus varies in inverse proportion to the arc length of the longitudinal slice at any point along the ray path. When the rays cross the detection area, we divide energy density by the extent of the detection area (5 km in our case) to convert to units of J/m^2. Subsequent division by Δf and Δt during the production of the spectrogram results in the appropriate units for power spectral density of W/m^2/Hz. We note that the precise value of the detection area is not critical so long as it remains within the bounds described above. If it is made larger, many more rays will cross it and will be divided by a larger area, thus yielding a similar power density, and vice versa.

2.3. Interpolation Between Sample Rays

[16] We now discuss the interpolation scheme that is used to generate a large number of rays in our simulation. As noted in section 2.2, the detection area through which rays must cross in order to be recorded onto the spectrogram is limited in spatial extent, in the present case to 5 km. Although this detection area is large compared with the physical dimensions of satellite-borne VLF electric field antennas (typically a few hundred meters tip to tip), it is nevertheless extremely small on magnetospheric scales, representing $\sim 8 \times 10^{-4}$ R_E, and consequently, the probability that a given ray will cross any given detection area is extremely small. Further, we have found that in order to produce well-defined, meaningful spectrograms, we need ~10,000 rays to cross the detection area, and when combined with the low probability of a single ray crossing the detection area, it is clear that we are required to simulate a very large number of rays, ~10–100 million, based on simple probabilistic arguments.

[17] Computing the ray paths of 100 million individual rays with the inclusion of Landau damping would take even the fastest computers a prohibitively long period of time. Fortunately, the general parameters associated with rays vary smoothly with wave frequency and injection latitude of the ray, thereby allowing us to appropriately sample the spatial extent and frequency spectrum of the lightning strike with a smaller number of rays (referred to as "sample rays") and interpolate the remainder of the rays between the sample rays.

[18] We illustrate our interpolation scheme in Figure 3, where we consider a lightning strike at 35° latitude and model the spreading in the Earth-ionosphere waveguide to be ±10° about the source, i.e. extending from 25° to 45°, sampled every 2° resulting in 11 rays for every frequency component. In Figure 3a we overlay the 2 kHz and 3 kHz frequency components (each frequency component having

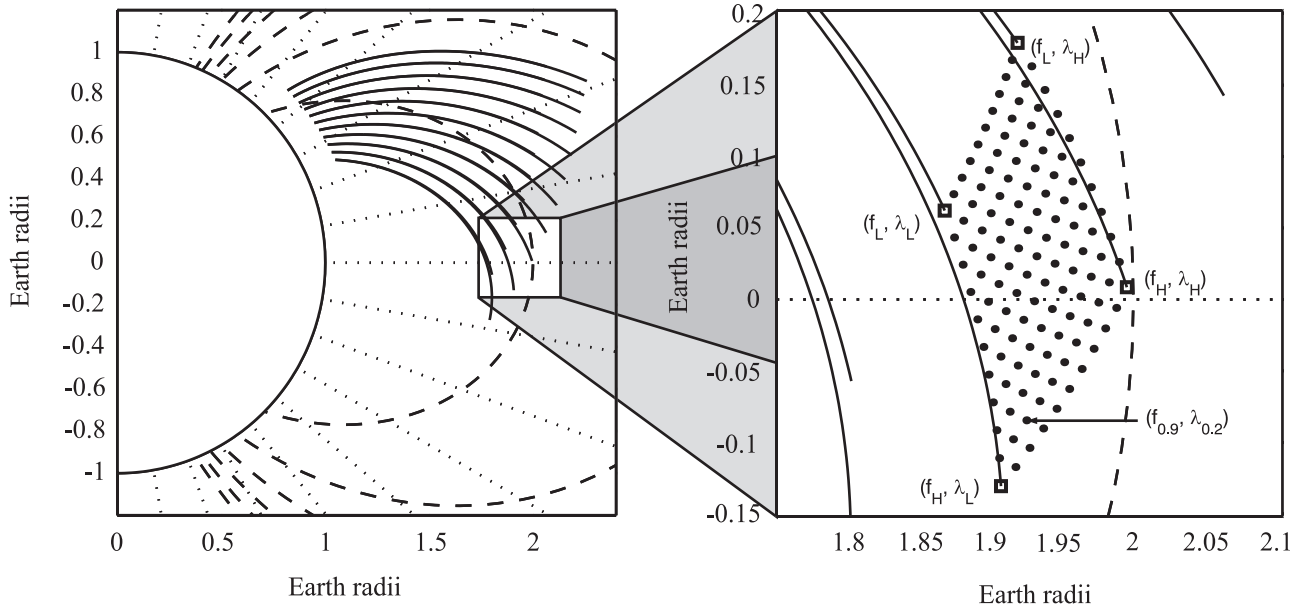

Figure 3. Interpolation scheme illustrated. (a) 2 kHz and 3 kHz frequency components overlaid at 0.3 s after the lightning strike, showing a ±10° latitudinal spread about the source at $\lambda_s = 35°$ and 11 rays per frequency component. (b) A blow-up of four adjacent rays, illustrating 100 interpolated rays, and an example of one interpolated ray with the nomenclature used in the text.

11 sample rays) and show an expanded plot of four adjacent sample rays and the interpolated rays in Figure 3b at 300 ms after the strike. We label the rays belonging to the lower frequency f_L and those of the higher frequency f_H, and similarly label the rays launched at the lower latitude and higher latitude λ_L and λ_H, respectively, and obtain the four guiding points (f_L,λ_L), (f_L,λ_H), (f_H,λ_L), (f_H,λ_H). If the frequencies and launch latitudes are chosen sufficiently close together (as outlined below), any interpolated ray of frequency f_i such that $f_L \leq f_i \leq f_H$ launched at a latitude λ_i such that $\lambda_L \leq \lambda_i \leq \lambda_H$ will be contained within the quadrilateral formed by the guiding points. Further, if we let m be a number between 0 and 1 representing the interpolated frequency f_i, where 0 corresponds to f_L and 1 corresponds to f_H, and similarly we let n be a number between 0 and 1 representing the interpolated launch latitude λ_i, 0 corresponding to λ_L and 1 corresponding to λ_H, than any interpolated quantity g_i can be obtained by the simple linear scaling

$$gi = a_1\, g(f_L,\lambda_L) + a_2\, g(f_L,\lambda_H) + a_3\, g(f_H,\lambda_L) + a_4\, g(f_H,\lambda_H), \tag{2}$$

where $a_1 = 1 - n - m - nm$, $a_2 = n - nm$, $a_3 = m - nm$, and $a_4 = nm$.

[19] Spatial interpolation is performed using λ and L-shell parameters since these give by far the most accurate and robust fits. Other interpolated quantities are ray energy and wave normal angle. It is also important to mention that interpolations are performed at certain fixed times in intervals of 0.4 ms, as if a snapshot of the traced rays was taken at some instant and all interpolated rays were found between the guiding points at that instant.

[20] The example shown in Figure 3 has very coarsely spaced sample rays for purposes of illustration. In our simulations we have chosen to sample the ±10° region about the source with rays spaced every 0.5° in latitude, resulting in 41 rays per frequency component. The assumed 200 Hz–60 kHz lightning frequency spectrum was sampled with 130 frequency components differing from each other by no more than 5%. The sampling process results in (130 × 41 =) 5330 sample rays. We have interpolated the latitude range at every 0.01° and the frequency spectrum at every 1 Hz, effectively resulting in ~120 million rays.

2.4. Landau Damping

[21] The Landau damping due to resonant interactions between whistler waves and suprathermal electrons was computed using the formulation of *Brinca* [1972] and a distribution function of suprathermal electrons given by

$$f(v) = 2 \times 10^5 / v^4 \left[\mathrm{cm}^{-6}\mathrm{s}^3\right]. \tag{3}$$

This distribution represents a numerical fit to flux measurements made with the HYDRA instrument on the POLAR satellite [*Bell et al.*, 2002], of electrons in the range 300 eV–10 keV, which are the energies of electrons most strongly involved in the Landau interaction. Landau damping, (or rather, the imaginary part of the $\boldsymbol{k}$-vector) was computed for all sample rays by evaluating equation (2) given by *Brinca* [1972] and integrating with respect to $v_\perp$ at each time step. Subsequent integration of k_{im} with respect to the distance traversed by the ray gives the variation of the wave power density along the ray path.

2.5. Construction of the Frequency-Time Spectrogram

[22] The frequency-time spectrogram is constructed by defining a two-dimensional array, with time and frequency as the abscissa and ordinate, respectively. The variables to choose are total duration, t_{max}, and highest frequency, f_{max}, for which the spectrogram will be constructed, as well as the

width of frequency and time bins, Δf and Δt. Using t_{max} and Δt, as well as f_{max} and Δf, we determine the number of bins required for each of the axes and hence the size of the array. Although Δf and Δt can, in principal, be chosen arbitrarily, they are bounded on the low end by the need to have $\Delta f \Delta t \geq 1$ and on the high end by a decrease in resolution of the resulting whistler traces. For our displays we use $\Delta t = 50$ ms and $\Delta f = 50$ Hz, resulting in $\Delta f \Delta t = 2.5$. Owing to the limited amount of space available in this paper, the spectrograms are necessarily made very small, and hence we have chosen Δf and Δt to be slightly larger than they need to be to aid visibility.

[23] The data obtained using the methodology outlined in section 2.2 is processed so that the wave energy represented by each ray is added into the appropriate *f-t* bin, and subsequently each bin is divided by Δf and Δt to give the correct units of W/m^2/Hz. The division by Δf and Δt is necessary to ensure that the correct average power appears at every Δf-Δt bin, regardless of the Δf and Δt values chosen for the creation of the particular spectrogram, and is consistent with the a priori integration of power-density with respect to frequency, space, and time at the injection point of the ray.

2.6. Plasmaspheric Medium

[24] The plasmaspheric medium through which rays are traced is modeled using a standard dipole model for the magnetic field, appropriate for our *L*-shells of interest ($L \leq 4$), and a cold plasma electron density based on the diffusive equilibrium formulation of *Angerami and Thomas* [1964]. The diffusive equilibrium model by itself does not give a steep enough radial decrease in density to match the typical profiles given by *Carpenter and Anderson* [1992], so a wide, one-sided duct is superimposed to implement the radial density profile shown in Figure 8a. This profile is a close fit to the profile given by *Carpenter and Anderson* [1992] for the conditions, $d = 0$, $t = 2$, $k_{pmax} = 4$, and $R = 90$. Other features shown in Figures 8c and 8d are obtained using one- or two-sided Gaussian ducts as described by *Bernhardt and Park* [1977] and spaced in accordance with occurrence statistics obtained from ISEE1 [*Ledocq et al.*, 1994]. These nonsmooth plasmaspheric density profiles are discussed in section 4.

2.7. Model Validation

[25] We have used many of the published MR whistler traces in our model validation process, and have found excellent agreement. The observations made aboard the Magion 4 and 5 satellites shown by *Shklyar and Jiříček* [2000] show well our predictions of both low and high latitude sources, and *Edgar* [1972] shows examples of MR whistlers produced by plasmaspheric density structures with a smooth portion below and a distorted portion above the whistler "nose frequency" as discussed in section 4.2 and shown in Figure 7.

[26] As an illustration, we have chosen to simulate perhaps the best-known MR whistler spectrogram from *Smith and Angerami* [1968], shown in Figure 2a. Following the analysis of *Edgar* [1972], we have used a standard diffusive equilibrium model, with an ionospheric composition at 1000 km altitude of 50% O^+ and 50% H^+ but have changed the temperature to 1380 K and the source altitude to 25°, since these values gave a better fit to the data, and have set our observing aperture to match the location of the satellite at $L = 2.4$, $\lambda = 5°$S. The simulation results are shown in Figure 2b, where we have also overlaid a scale outline of the MR whistler of Figure 2a. As can be seen, the model is able to reproduce the timing of the observed spectrogram very accurately. Since the power levels aboard OGO 1 were controlled by an AGC, the lower portion of component 2 is suppressed owing to the arrival of the more intense "nose" of component 3. In addition, the observed spectrogram overlays the most intense (red) portions of our simulated spectrograms as would be expected. Beyond ~3 s, the observed MR whistler seems to decay faster than what our model predicts, which could be an indication that suprathermal particle fluxes were perhaps somewhat higher on this day (leading to more rapid Landau damping) than our assumed average values (we have made no effort to replicate the damping rate in this example) or alternatively that the satellite has moved into a more electromagnetically noisy environment where the AGC has suppressed the whistler signal. Since the output voltage of the receiver is not available to us, we cannot determine the source of this discrepancy.

3. Smooth Plasmasphere

[27] We begin by presenting results for the case of a smooth plasmasphere with a plasmapause at $L = 3.8$ as shown in Figure 4. The electron density profile is as given in Figure 8a and is fitted to the model profile of *Carpenter and Anderson* [1992] as discussed above.

[28] The columns in Figure 4 represent observations arising from a given lightning strike source latitude, from left to right $\lambda_s = 25°$, 35°, 45°, and 55°, while the rows represent particular observation locations along the magnetic equatorial plane of waves arising from lightning strikes at different source latitudes, from top to bottom $L = 2$, 2.5, 3, 3.5, and 4. In the following discussion we briefly review the general dispersion characteristics observed by previous workers and then focus our attention on wave power damping, spatial dispersion, and some other peculiar features particular to the case in hand.

3.1. General Observations

[29] When viewing the power distribution of whistler waves in the plasmasphere as in Figure 4, certain features are readily apparent: the first is that the radiation is very strongly contained within the plasmasphere, and even though some energy leaks out beyond the plasmapause to $L = 4$, the wave power levels are generally 30–60 dB weaker in this region, compared with the region immediately within the plasmapause at $L = 3.5$. The frequency range occupied by the whistlers moves to lower frequencies with increasing *L*-shell of the observation location owing to the general tendency of ray paths to settle on those *L*-shells where the wave frequency is approximately equal to the equatorial lower hybrid resonance (LHR) frequency [*Shklyar and Jiříček*, 2000; *Ristic'-Djurovic' et al.*, 1998].

[30] Whistlers at low *L*-shells tend to have a well-defined lower cutoff frequency owing to the combination of the lightning source latitude, the limited injection latitude range [*Edgar*, 1976], and tendency of the lower frequency components to propagate to higher *L*-shells [*Draganov et al.*, 1992]. Such behavior was recently documented with obser-

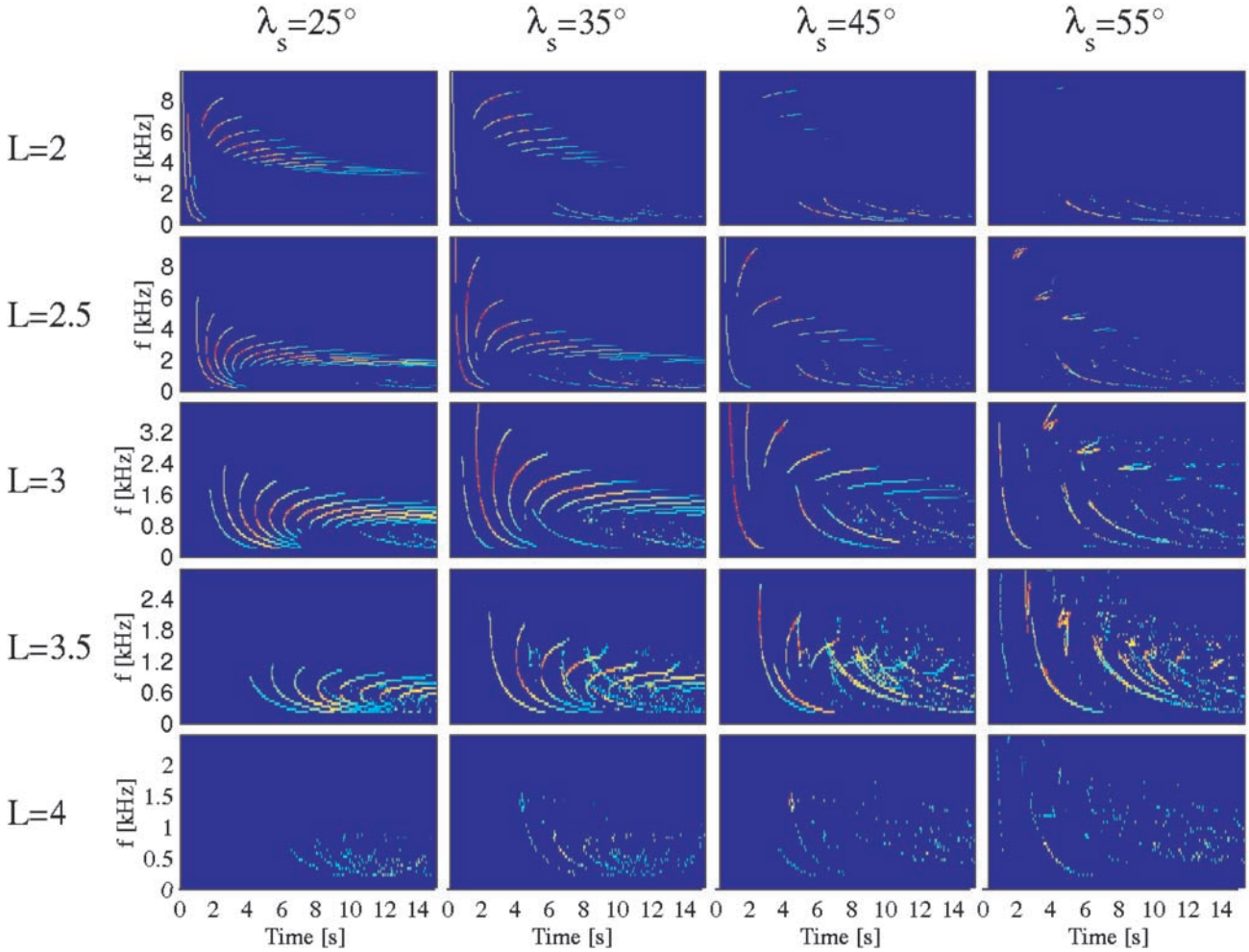

Figure 4. The *f-t* spectrograms in a smooth plasmasphere (see Figure 8a), showing the lightning strike latitude at the top of each column, from left to right $\lambda_s = 25°$, 35°, 45°, and 55°, and observation location across each row, from top to bottom $L = 2$, 2.5, 3, 3.5, and 4. The common color bar is shown in Figure 7.

vations aboard the Magion 4 and 5 spacecraft [*Shklyar and Jiříček*, 2000].

[31] The frequency band occupied by the whistlers (particularly toward the beginning of the spectrogram) increases with increasing lightning source latitude, as does the time between subsequent hops. As discussed by *Shklyar and Jiříček* [2000] and noted by *Smith and Angerami* [1968], the nose frequency (i.e., the frequency of minimum group delay) of the MR whistler tends to decrease with time and is also lower for lower lightning source latitudes. Somewhat puzzling features of whistler propagation can be seen in the traces for $\lambda_s = 45°$ and $\lambda_s = 55°$, at $L = 3.0$ and 3.5, where we note the additional presence of lower-frequency components having seemingly unrelated dispersion characteristics and appearing at irregular times. In addition, the $\lambda_s = 55°$ case shows high-frequency components at $L = 2.5$ and $L = 3.0$ with peculiar dispersion characteristics. These features are due largely to reflections from the plasmapause boundary and are discussed further in section 3.3.

3.2. Power Damping and Spatial Dispersion

[32] In examining the power and duration of MR whistlers for the case of $\lambda_s = 25°$ in Figure 4, we note that at low *L*-shells of observation the wave power diminishes more rapidly than at higher *L*-shells. We show in Figures 7a and 7b the plots for $\lambda_s = 25°$, $L = 3.0$ and $L = 3.5$, respectively, similar to the corresponding plots of Figure 4 but with a 60 s timescale to emphasize the longevity of the whistler waves at these high *L*-shells of observation. Note that the frequency band occupied by the whistlers diminishes with time, and the frequency component that tends to settle at a given *L*-shell (i.e., the "settling frequency") is lower at higher *L*-shells. As noted above, the wave power persists for a longer time at $L = 3.5$ than at $L = 3$. The intensity of the whistler waves, however, tends to decrease with increasing *L*-shells. We note again from Figure 4 that in the $\lambda_s = 25°$, $L = 2.0$ panel, 6 MR whistler components had intensities in the range −20 to −30 dB (dB is given relative to 1 pW/m^2/Hz), whereas the $\lambda_s = 25°$, $L = 3.5$ panel had no whistler waves with intensities in this range.

[33] These observations are consistent with the findings of *Bortnik et al.* [2002], who have noted that there is a competition between increased lifetimes of MR whistlers at higher *L*-shells and higher initial power spectral density for MR components settling at lower *L*-shells, resulting in an MR whistler energy deposition maximum in the vicin-

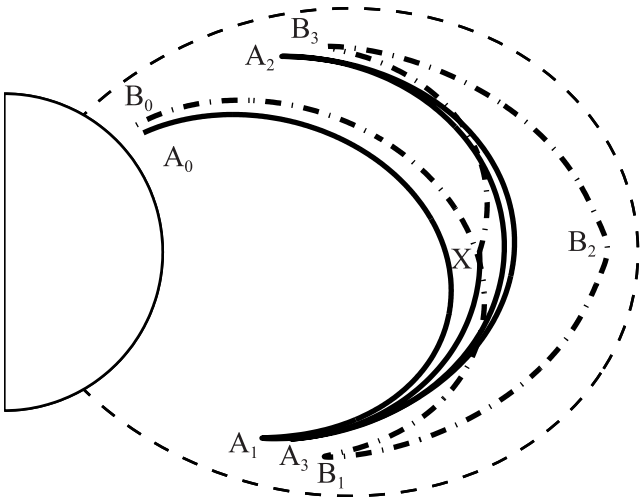

Figure 5. Ray tracings showing plasmapause echo traces, in particular Figure 4, $\lambda_s = 45°$, $L = 3$, at $t = 5$ s. Ray A has $f = 2.523$ kHz, $\lambda = 40.6°$ and approaches the satellite location (X) without plasmapause reflection. Ray B has $f = 1.088$ kHz, $\lambda = 43.9°$ and reflects off the plasmapause at B_2.

ity of the slot-region between the inner and outer radiation belts.

[34] We note that the tendency for longer lifetimes of MR whistler components at higher L-shells, and higher wave power intensities at lower L-shells seems to be independent of the lightning injection latitude as seen from the $\lambda_s = 35°$, $\lambda_s = 45°$, and $\lambda_s = 55°$ columns in Figure 4. Figures 6 and 7 also indicate that this trend is also largely independent of ionospheric and plasmaspheric electron density structures.

3.3. Peculiar Frequency-Time Features

[35] Referring to Figure 4 once again, we note that in addition to the expected MR components, there are additional features that appear, such as those which can be seen for $\lambda_s = 35°$ and 45°, at $L = 3.0$ and 3.5. These features are largely due to reflections from the plasmapause boundary. To demonstrate that this is the case, we ran the $\lambda_s = 35°$ and 45° cases with the plasmapause moved out to $L = 5.6$ simulating the conditions where $k_{pmax} = 0$ (in the previous 24 hours) or very quiet conditions, as shown by the electron density profile in Figure 8b. The results shown in Figure 6, columns 1 and 2 show that the MR traces are now "smooth" and follow the same trend as at lower L-shells. To illustrate how this happens, we examine the reflection process from the plasmapause, and we examine the case shown in Figure 4, for $\lambda_s = 45°$, at $L = 3.0$. Looking at a snapshot at $t = 5$ s, two seemingly unrelated frequency branches seem to coexist, one at $2.1 \leq f \leq 2.6$ and another at $0.2 \leq f \leq 2.0$. We choose the two frequencies at $t = 5$ s and show in Figure 5 the origin of the two whistler branches.

[36] The ray labeled A is the 2.523 kHz component and is injected at $\lambda = 40.6°$ at A_0, undergoes magnetospheric reflections at A_1, A_2, and A_3, and then crosses the detection area marked X at $t = 5$ s. In a similar way, the ray labeled B is the 1.088 kHz component and is injected at $\lambda = 43.9°$ at B_0. The ray then undergoes a MR at B_1, but as it moves to higher L-shells, it encounters the plasmapause at $L = 3.8$ (B_2) and is reflected back into the plasmasphere. It then undergoes another MR at B_3 and finally crosses the detection area (X) at $t = 5$ s. When the plasmapause is moved to higher L-shells, such plasmapause echoes are eliminated, resulting in traces such as the ones shown in Figure 6, columns 1 and 2.

[37] The hook-like features (resembling the letter "h") shown in Figure 4, $\lambda_s = 55°$, $L = 2.5$ and 3.0 result in the same way, owing to plasmapause reflections. Notice that despite the unusual trajectories of these echoes, they nevertheless result in smooth, continuous f-t features.

4. Nonsmooth Plasmaspheres

[38] The results presented in the previous section were for a plasmasphere with a smooth density profile, plasmapause located at either $L = 3.8$, or 5.6, and rays launched with vertical wave normal angles at an altitude of 1000 km. While the real plasmasphere (and ionosphere) can on occasion be relatively smooth, it is also known to support field-aligned density structures such as ducts [*Bernhardt and Park*, 1977; *Smith and Angerami*, 1968] or ledges [*Edgar*, 1976]. The ionosphere can also have irregularities or horizontal density gradients that cause latitude- and frequency-dependent refraction of the rays as they traverse the ionosphere, so that the wave normal angles may not necessarily be vertical at the injection point. In this section we consider the effect of various density irregularities on the f-t signatures, recorded at various locations in the plasmasphere. We choose three representative cases to study: an irregular, randomizing ionosphere, a ducted plasmasphere, and a ledged plasmasphere, and we only examine a subset of lightning source latitudes for the purposes of brevity.

4.1. Randomizing Ionosphere

[39] To study the effects of many small-scale irregularities in the ionosphere, together with larger-scale horizontal density gradients, we perform a simulation similar to that discussed in section 3 with a smooth plasmasphere (Figure 8a) but randomize the wave normal angle at the injection point of the ray. In other words, each of the 5330 sample rays (130 frequency components and 41 latitude locations per frequency) are assigned a random number for their initial wave normal angles, uniformly distributed between $-30°$ and 30° about the local vertical direction. Though such wave normal cones have been shown to exist [*James*, 1972], it is more common that all wave normal angles at a particular location will be bent somewhat uniformly, generally resulting in a much smaller cone centered on a particular wave normal direction. Our choice of completely random initial wave normal angles thus represents the extreme situation with dramatic ionospheric wave normal randomization. Also, it is important to note that the spectrograms are constricted with $\Delta f = 50$ Hz, whereas the rays are interpolated at every 1 Hz, and consecutive sample rays are typically 10–100 Hz apart in frequency. Thus each Δf-Δt bin in the spectrograms shown records a large number of rays with randomized wave normal angles.

[40] The results for lightning source latitude of $\lambda_s = 25°$ and $\lambda_s = 35°$ are shown in Figure 6, columns 3 and 4. We observe that even with such scattered initial wave normals, there are well-defined f-t features observable in the spectro-

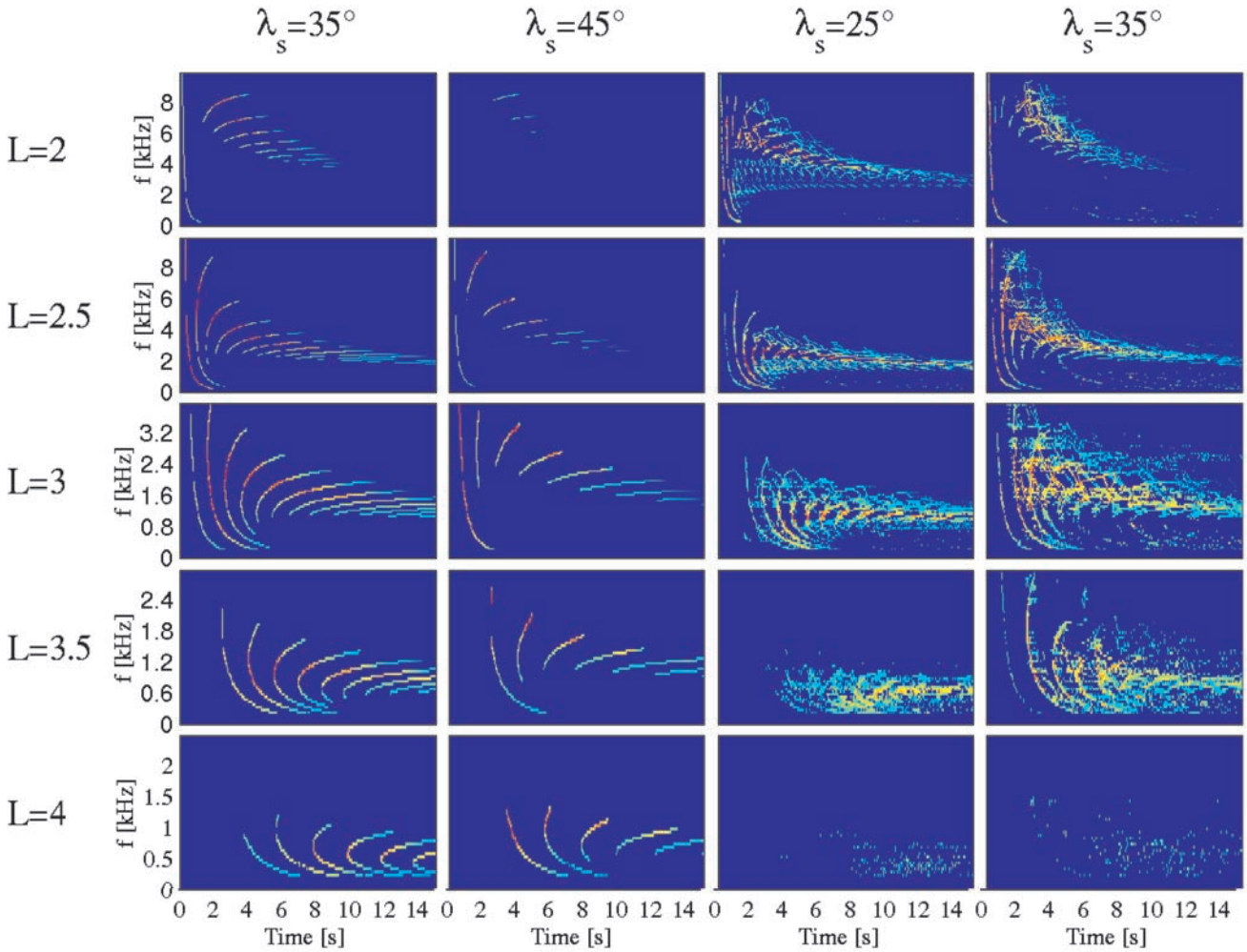

Figure 6. The *f-t* spectrograms presented in the format of Figure 4. Columns 1 and 2 are computed using a smooth plasmasphere on a quiet day (see Figure 8b) for $\lambda_s = 35°$ and 45°, and columns 3 and 4 are computed using a randomizing ionosphere for $\lambda_s = 25°$ and 35°. The common color bar is shown in Figure 7.

gram, having all the general features discussed in section 3, such as a nose-frequency, *L*-shell dependent damping rates, and frequency separation in accordance with equatorial LHR frequency. The marked difference to the corresponding plots in Figure 4 is that the sharply defined MR whistler components evolve into an incoherent noise band far more quickly. The upper and lower cutoff frequencies of the MR trace are similar to the smooth case but are more diffuse. The higher frequency components, particularly in the $\lambda_s = 35°$, $L = 3.0$ case, become incoherent very rapidly. Damping rates show the characteristic trends discussed in section 3.2.

4.2. Ducted Plasmasphere

[41] To simulate an irregular plasmasphere, we inject rays at 1000 km altitude with vertical wave normal angles, but instead of using the smooth plasmasphere of Figure 8a, we superpose eight two-sided ducts of 30% enhancement as shown in Figure 8c, spaced roughly according to the statistics presented for real whistler duct observations aboard the ISEE spacecraft [*Ledocq et al.*, 1994]. The density enhancement of the duct exponentially rises from 0% at the Earth's surface to its full value of 30% at an altitude of 1500 km. Using this plasmaspheric profile we examine the observations MR components produced by a lightning strike at $\lambda_s = 25°$ and briefly mention the differences due to lightning strikes at higher latitudes (not shown). From Figure 7, column 1, we see that whistler energy is primarily confined to the plasmasphere, with very little energy leaking out to $L = 4$ as in the smooth plasmasphere. The frequency bands observed at each *L*-shell are also surprisingly consistent with those of nonducted whistlers, indicating that the majority of whistler wave energy is not trapped by the enhancement ducts. The lifetimes at each *L*-shell are consistent with those of the smooth plasmasphere.

[42] An interesting feature in Figure 7 becomes apparent if we examine the *f-t* signature of the MR whistlers above and below the nose frequency. We see from observations at $L = 3.0$ and $L = 3.5$ that for frequency components below the nose frequency, the MR whistler remains coherent, well defined, and similar in appearance to the case of the smooth plasmasphere in Figure 4. However, the portions of the MR whistlers at frequencies above the nose frequency appear

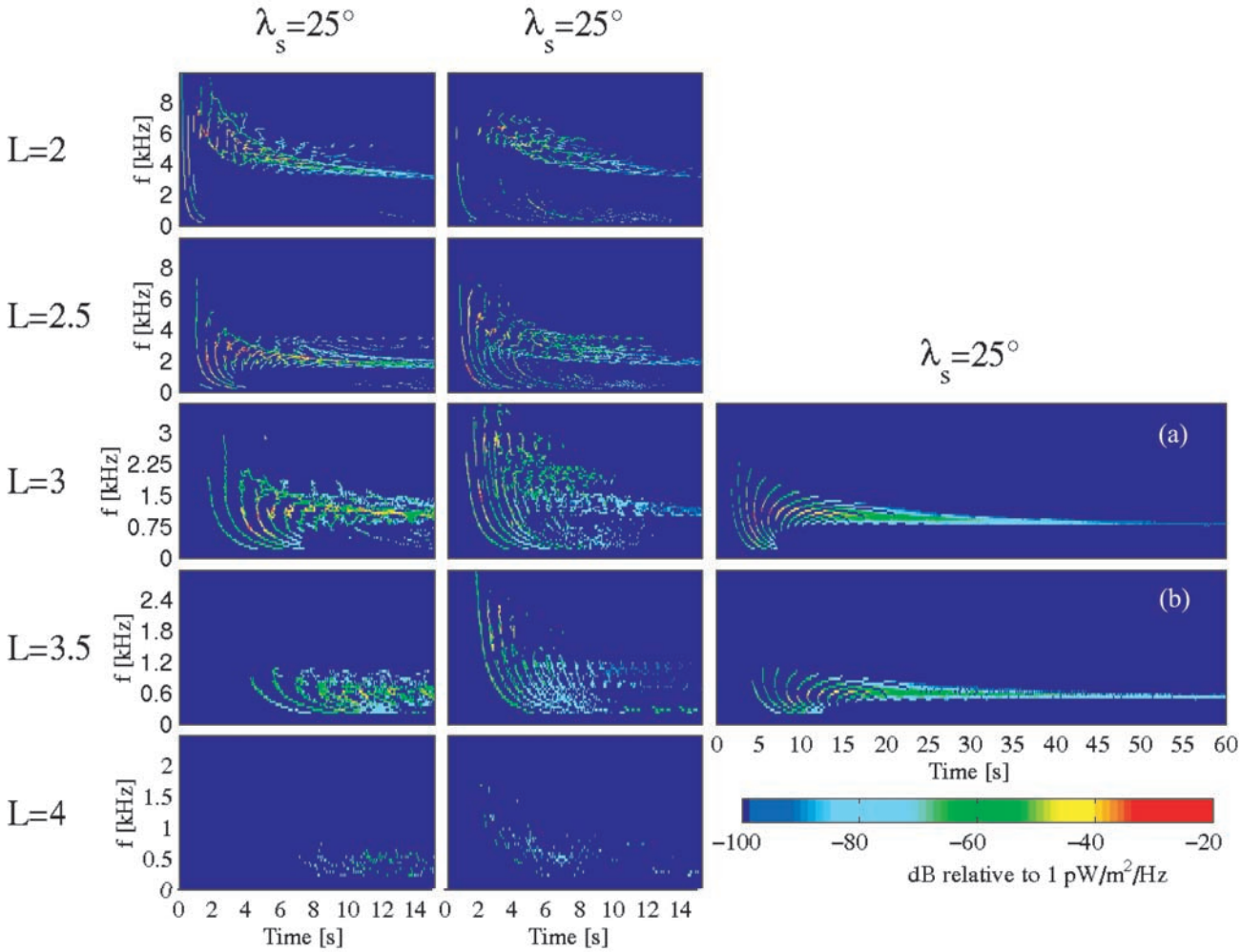

Figure 7. The *f-t* spectrograms presented in the format of Figure 4. Column 1 shows the results for a plasmasphere permeated by eight two-sided 30% enhancement ducts (see Figure 8c) when $\lambda_s = 25°$, Column 2 shows a similar plasmasphere but the ducts are one-sided (see Figure 8d). (a–b) The results for a smooth plasmasphere (Figure 8a) for $\lambda_s = 25°$ and $L = 3$ and 3.5, with an extended timescale to show lifetime variation. The common color bar used in all spectrograms is shown in units of dB relative to 1 pW/m^2/Hz.

incoherent, randomized, and are not similar to their counterparts in Figure 4. To explain this somewhat peculiar behavior, we note that the nose frequency of the MR whistler lies very close to the LHR frequency of that particular *L*-shell, and it is the latter frequency which plays a key role in the behavior of the *f-t* trace. Following the analysis of *Helliwell* [1965] for whistler waves below $f_H/2$ we see that for ducted propagation (where the duct is an enhancement duct or "crest") the wave normal angle must remain within a small cone about the static magnetic field direction. Since our waves do not start out in the duct and have initial wave normal angles well outside the trapping cone, we expect these waves to go through the ducted plasmasphere with little influence from the ducts, which is indeed the case for $f < f_{LHR}$. However, when $f \geq f_{LHR}$ the refractive index surface becomes "open" and a minimum appears at the Gendrin angles [*Helliwell*, 1965, Figures 3–17]. For whistlers with wave normal angles near the Gendrin angle, trapping in field-aligned depletions (troughs) is possible, since the ray and wave normal point in opposite sense about the static magnetic field. In our model plasmasphere the outer edges of the crests appear as one sided troughs which are able to partially guide or at least distort the otherwise smooth trajectories of whistler waves with $f \geq f_{LHR}$, whereas for $f < f_{LHR}$, this possibility does not exist and the ray paths are almost entirely unaffected by the presence of the ducts. This result suggests that MR whistlers observed on satellites with smooth $f \leq f_{LHR}$ and distorted or randomized for $f \geq f_{LHR}$ components can be used as strong indicators of the presence of one or more enhancement ducts.

4.3. Ledged Plasmasphere

[43] We now study the effects of a plasmasphere striated with one-sided ducts or electron density ledges by converting the two-sided ducts of Figure 8c to one-sided ducts (shown in Figure 8d), keeping the distribution and locations of the ducts unchanged.

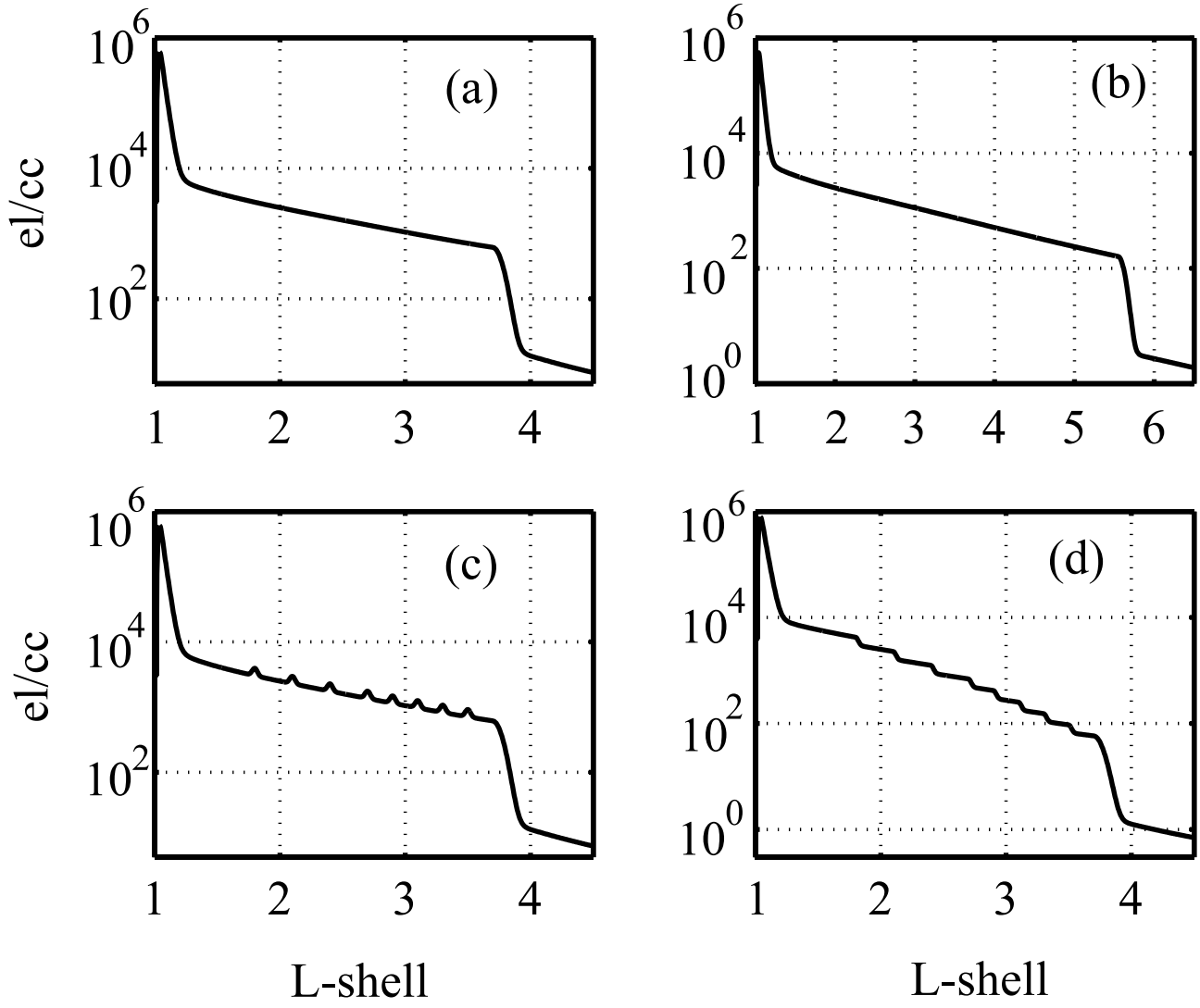

Figure 8. Panels showing the equatorial electron density profile in el/cc as a function of *L*-shell, for (a) a smooth plasmasphere under typical conditions, $K_p = 4$, $L_K \approx 3.8$, (b) a smooth plasmasphere under quiet conditions, $K_p = 0$, $L_K \approx 5.6$, (c) a nonsmooth plasmasphere with eight two-sided 30% enhancement ducts, and (d) a nonsmooth plasmasphere as in Figure 8c but with one-sided instead of two-sided ducts.

[44] We show in Figure 7, column 2 the observed spectrograms resulting from a lightning strike latitude of $\lambda_s = 25°$. Again, the wave energy is confined to the plasmasphere with very weak traces barely visible at $L = 4.0$. The frequency bands that are prevalent in Figure 4, column 1 are only weakly present in this simulation, and the lifetime of the whistler wave trains is dramatically shortened.

[45] Perhaps the most notable feature in this spectrogram is the absence of a nose frequency and the much reduced effects of dispersion between subsequent MR whistler components. Both of the above features are attributed to the stronger guiding potential of one-sided ducts and the fact that whistler waves in this spectrogram are predominantly confined to lower wave normal angle values. We note in passing that lightning source latitudes of $\lambda_s \geq 35°$ (not shown) result in only the first and second whistler hops visible on the spectrograms at all *L*-shells of observation. Beyond that, wave energy leaks out into the Earth-ionosphere waveguide and is eliminated from further plasmaspheric propagation.

5. Summary and Conclusions

[46] We have used a numerical method to simulate the population of the plasmasphere by MR whistlers, allowing the determination of the observed *f-t* spectrogram at a given location in the plasmasphere, resulting from a lightning strike at any given latitude on Earth. Using a two-dimensional ray tracing code we calculate the trajectories of 5330 whistler rays that effectively sample the lightning strike's frequency spectrum and latitudinal spread about the source, and then use these so-called "sample rays" to create ~120 million interpolated rays. Each ray is appropriated a measure of energy according to its frequency and injection latitude, and this energy is progressively attenuated along the ray's trajectory using a Landau damping calculation with realistic

suprathermal electron fluxes. An equatorial detection area is defined to illustrate what would be observed on a satellite, and the rays that cross it are recorded and subsequently used to construct the final *f-t* spectrogram.

[47] Using the technique described above, we studied the effect upon the appearance of the *f-t* spectrogram, of changing the observation location in the plasmasphere (L = 2, 2.5, 3, 3.5, and 4), the location of the lightning strike (λ_s = 25°, 35°, 45°, and 55°), and the underlying plasmaspheric and ionospheric density structures.

[48] Our results quantify the effects that all three factors (observation location, source latitude, and plasmaspheric density) have on the appearance of whistler waves in the simulated spectrograms. As the observation location is moved further away from the Earth, the frequency band in which MR whistler waves appear moves to lower frequencies, the intensity of the whistler wave components diminishes, and the lifetime of the whistler echo train is increased such that at L = 3.5, wave energy can exist for tens of seconds before being absorbed by the suprathermal plasma.

[49] As the lightning strike latitude is increased, we find that the time interval between MR whistler echoes increases and that the frequency band occupied by the whistlers at every observation point is higher. In addition, we have found that at higher lightning strike latitudes there are whistler components reflecting off the plasmapause and appearing as distinct traces with a unique dispersion characteristic on the *f-t* spectrograms.

[50] We have simulated an ionosphere that strongly randomizes the wave normal angle of the whistler wave during the trans-ionospheric passage and found that MR whistlers appeared well defined in the first few hops but quickly evolved into an incoherent noise band. The case of a plasmasphere permeated by field-aligned structures again showed distinctive behavior indicative of the nature of the field-aligned density structure.

[51] In conclusion, we have showed that the MR whistler echo train carries with it a great deal of information about the location of the causative lightning strike, the exact location in the plasmasphere where it was recorded, and of course, the electron density structure of the intervening plasmaspheric medium. Given the distinctive effects that each of these parameters has on the appearance of the *f-t* spectrograms, it should be possible to crudely infer the structure of the cold plasma in the plasmasphere, lightning strike latitude, and observation location of the *f-t* spectrogram. Though we have not explicitly investigated the effects of varying fluxes of suprathermal electrons in this work, it is possible that information on the electron distribution may also be obtained from the lifetimes of observed MR whistler echo trains.

[52] **Acknowledgments.** This research was supported by the Air Force Office of Scientific Research under grant F49620-99-1-0339-P00001, as well as by NASA grant NAS5-30371 via subcontract from the University of Iowa.

[53] Arthur Richmond thanks J. Bernard Blake and Steven Cummer for their assistance in evaluating this paper.

References

Angerami, J. J., and J. O. Thomas, Studies of planetary Atmospheres, 1, The distribution of electrons and ions in the Earth's exosphere, *J. Geophys. Res.*, *69*, 4537, 1964.

Bell, T. F., U. S. Inan, J. Bortnik, and J. D. Scudder, The Landau damping of magnetospherically reflected whistlers within the plasmasphere, *Geophys. Res. Lett.*, *29*(15), 1733, doi:10.1029/2002GL014752, 2002.

Bernhardt, P. A., and C. G. Park, Protonospheric-ionospheric modeling of VLF ducts, *J. Geophys. Res.*, *82*, 5222, 1977.

Blake, J. B., U. S. Inan, M. Walt, T. F. Bell, J. Bortnik, D. L. Chennette, and H. J. Christian, Lightning-induced energetic electron flux enhancements in the drift loss cone, *J. Geophys. Res.*, *106*, 29,733, 2001.

Bortnik, J., U. S. Inan, and T. F. Bell, *L*-dependence of energetic electron precipitation driven by magnetospherically reflecting whistler waves, *J. Geophys. Res.*, *107*(A8), 1150, doi:10.1029/2001JA000303, 2002.

Brinca, A. L., On the stability of Obliquely propagating whistlers, *J. Geophys. Res.*, *77*, 3495, 1972.

Carpenter, D. L., and R. R. Anderson, An ISEE/Whistler model of equatorial electron density in the magnetosphere, *J. Geophys. Res.*, *97*, 1097, 1992.

Crary, J. H., The effect of the Earth-ionosphere waveguide on whistlers, *Tech. Rep. 9*, Radioscience Lab., Stanford Electron. Lab., Stanford Univ., Stanford, Calif., 1961.

Cummer, S. A., and U. S. Inan, Measurement of charge transfer in sprite producing lightning using ELF radio atmospherics, *Geophys. Res. Lett.*, *24*, 1731, 1997.

Draganov, A. B., U. S. Inan, V. S. Sonwalker, and T. F. Bell, Magnetospherically reflected whistlers as a source of plasmaspheric hiss, *Geophys. Res. Lett.*, *19*, 133, 1992.

Draganov, A. B., U. S. Inan, V. S. Sonwalker, and T. F. Bell, Whistlers and plasmaspheric hiss: Wave directions and three-dimensional propagation, *J. Geophys. Res.*, *98*, 11,401, 1993.

Edgar, B. C., The structure of the magnetosphere as deduced from magnetospherically reflected whistlers, *Tech. Rep. 3438-2*, Radiosc. Lab., Stanford Electron. Lab., Stanford Univ., Stanford, Calif., 1972.

Edgar, B. C., The upper- and lower-frequency cutoffs of magnetospherically reflected whistlers, *J. Geophys. Res.*, *81*, 205, 1976.

Helliwell, R. A., *Whistlers and Related Ionospheric Phenomena*, Stanford Univ. Press, Stanford, Calif., 1965.

Inan, U. S., and T. F. Bell, The plasmapause as a VLF waveguide, *J. Geophys. Res.*, *82*, 2819, 1977.

Inan, U. S., H. C. Chang, and R. A. Helliwell, Electron precipitation zones around major ground-based VLF signal sources, *J. Geophys. Res.*, *89*, 2891, 1984.

James, H. G., Refraction of whistler-mode waves by large-scale gradients in the middle latitude ionosphere, *Ann. Geophys.*, *28*, 301, 1972.

Jasna, D., U. S. Inan, and T. F. Bell, Precipitation of suprathermal (100 eV) electrons by oblique whistler waves, *Geophys. Res. Lett.*, *19*, 1639, 1992.

Johnson, M. P., U. S. Inan, and D. S. Lauben, Subionospheric VLF signatures of oblique (nonducted) whistler-induced precipitation, *Geophys. Res. Lett.*, *26*, 3569, 1999.

Kimura, I., Effects of ions on whistler-mode ray tracing, *Radio Sci.*, *1*, 269, 1966.

Lauben, D. S., U. S. Inan, and T. F. Bell, Poleward-displaced electron precipitation from lightning-generated oblique whistlers, *Geophys. Res. Lett.*, *26*, 2633, 1999.

LeDocq, M. J., D. A. Gurnett, and R. R. Anderson, Electron number density fluctuations near the plasmapause observed by the CRRES spacecraft, *J. Geophys. Res.*, *99*, 23,661, 1994.

Ristic'-Djurovic', J. L., T. F. Bell, and U. S. Inan, Precipitation of radiation belt electrons by magnetospherically reflecting whistlers, *J. Geophys. Res.*, *103*, 9249, 1998.

Shklyar, D. R., and F. Jiříček, Simulation of nonducted whistler spectrograms observed aboard the Magion 4 and 5 Satellites, *J. Atmos. Sol. Terr. Phys.*, *62*, 347, 2000.

Smith, R. L., and J. J. Angerami, Magnetospheric properties deduced from OGO 1 observations of ducted and nonducted whistlers, *J. Geophys. Res.*, *73*, 1, 1968.

Sonwalker, V. S., and U. S. Inan, Wave normal direction and spectral properties of whistler mode hiss observed on the DE 1 satellite, *J. Geophys. Res.*, *93*, 7493, 1988.

Thorne, R. M., and R. B. Horne, Landau damping of magnetospherically reflected whistlers, *J. Geophys. Res.*, *99*, 17,249, 1994.

Uman, M. A., *Lightning*, Dover, Mineola, N.Y., 1984.

T. F. Bell, J. Bortnik, and U. S. Inan, Space, Telecommunications, and Radioscience Laboratory, Electrical Engineering Department, Stanford University, Packard 355, MC 9515, 350 Serra Mall, Stanford, CA 94305-9515, USA. (bell@nova.stanford.edu; jbortnik@stanford.edu; inan@nova.stanford.edu)